Hierarchical structures in Northern Hemispheric extratropical winter ocean-atmosphere interactions

Marc Wiedermann[*1,2], Jonathan F. Donges[1,3], Dörthe Handorf[4], Jürgen Kurths[1,2,5,6], and Reik V. Donner[1]

[1]Potsdam Institute for Climate Impact Research — P.O. Box 60 12 03, 14412 Potsdam, Germany, EU
[2]Department of Physics, Humboldt University — Newtonstr. 15, 12489 Berlin, Germany, EU
[3]Stockholm Resilience Centre, Stockholm University — Kräftriket 2B, 114 19 Stockholm, Sweden, EU
[4]Alfred Wegener Institute, Helmholtz Centre for Polar and Marine Research — Telegrafenberg A43, 14473 Potsdam, Germany
[5]Institute for Complex Systems and Mathematical Biology, University of Aberdeen — Aberdeen AB24 3FX, UK, EU
[6]Department of Control Theory, Nizhny Novgorod State University —

November 15, 2016

Abstract

In recent years extensive studies on the Earth's climate system have been carried out by means of advanced complex network statistics. The great majority of these studies, however, have been focusing on investigating correlation structures within single climatic fields directly on or parallel to the Earth's surface. Here, we develop a novel approach of node weighted coupled network measures to study correlations between ocean and atmosphere in the Northern Hemisphere extratropics and construct 18 coupled climate networks, each consisting of two subnetworks. In all cases, one subnetwork represents monthly sea-surface temperature (SST) anomalies, while the other is based on the monthly geopotential height (HGT) of isobaric surfaces at different pressure levels covering the troposphere as well as the lower stratosphere. The weighted cross-degree density proves to be consistent with the leading coupled pattern obtained from maximum covariance analysis. Network measures of

---

[*]marcwie@pik-potsdam.de

higher order allow for a further analysis of the correlation structure between the two fields and consistently indicate that in the Northern Hemisphere extratropics the ocean is correlated with the atmosphere in a hierarchical fashion such that large areas of the ocean surface correlate with multiple statistically dissimilar regions in the atmosphere. Ultimately we show that, this observed hierarchy is linked to large-scale atmospheric variability patterns, such as the Pacific North American pattern, forcing the ocean on monthly time scales.

Keywords: coupled climate networks, extratropical ocean-atmosphere interaction, node-weighted network measures, hierarchical networks

1 Introduction

In the last years, complex network analysis has been established as a powerful tool to study statistical interdependencies in the climate system (Donges et al. 2009a; Donges et al. 2015a; Tsonis and Roebber 2004; Tsonis et al. 2006; Tsonis et al. 2008). Links in the so-called climate networks represent functional interdependencies indicated by significant correlations (Donges et al. 2009a; Donges et al. 2009b; Paluš et al. 2011; Radebach et al. 2013) or the synchronous occurrence of extreme events (Boers et al. 2013; Boers et al. 2014b; Malik et al. 2010; Malik et al. 2011; Stolbova et al. 2014) in climatic time series taken at different grid points or measurement sites on or parallel to the Earth's surface.

In addition to studies on observational data of climate dynamics, climate networks have also been applied successfully to hindcast extreme events, such as extreme precipitation in South America (Boers et al. 2014a), or to predict the occurrence of El Niño episodes (Ludescher et al. 2013; Ludescher et al. 2014) and discriminate between different event types (Radebach et al. 2013; Tsonis and Swanson 2008; Wiedermann et al. 2016; Yamasaki et al. 2008).

So far, most studies conducted within the framework of climate networks focused solely on the dynamics within a single climatic field or layer. Besides atmospheric characteristics like surface air temperature, sea level pressure, or precipitation, recent studies have also addressed ocean dynamics represented by ocean temperature variability at the surface (Feng and Dijkstra 2014; Tantet and Dijkstra 2014) or different depths (Mheen et al. 2013) as well as the spatio-temporal variability in the strength of the Atlantic meridional overturning circulation (Feng et al. 2014).

It is well known, however, that the dynamics within the two major subcomponents of the Earth's climate system, ocean and atmosphere, are closely entangled (Frankignoul et al. 2001; Trenberth and Hurrell 1994). Examples for these interrelationships include the North Atlantic eddy-driven jet stream (Woollings et al. 2010) or the Pacific ocean forcing to the atmosphere which is closely related to the dynamics of the El Niño Southern Oscillation (Wyrtki 1975). Further, it has been shown that on time scales of up to one month the ocean is forced by atmospheric circulation, prominently manifested in terms of long-term variability patterns like the Pacific North American pattern (e.g. Frankignoul and Sennchael 2007) and the North Atlantic Oscillation (Czaja and Frankignoul 1999; Gastineau and Frankignoul 2015).

Inspired by approaches to investigate the interaction structure between different mutually coupled subsystems such as infrastructure networks (Boccaletti et al. 2014; Buldyrev et al. 2010; Vespignani 2010) a novel set of coupled network measures has been proposed by Donges et al. (2011) which provides a general tool to quantify interdependencies between subcomponents in complex coupled climate networks. The latter framework has been successfully applied to investigate interactions between different layers of geopotential height fields, where each isobaric surface forms a subcomponent of a larger climate network. Similarly, coupled climate networks have been constructed to study ocean-atmosphere interactions in the tropical Pacific (Feng et al. 2012) or over the South Atlantic Convergence Zone (Tirabassi et al. 2015).

Following upon these previous studies, in this work we extend the approach by Donges et al. (2011) and present an exploratory study to understand and quantify ocean-atmosphere interactions in the Northern Hemisphere mid-to-high latitudes during boreal winter at monthly scales. This temporal restriction is chosen, since previous studies by means of lagged maximum covariance analysis (MCA) have already revealed that the statistical interrelationship between atmosphere and ocean is strongest and most significant at lags of zero or one month during late fall and winter (e.g. Czaja and Frankignoul 1999; Frankignoul and Sennchael 2007; Gastineau and Frankignoul 2015; Liu et al. 2006; Wen et al. 2005).

To investigate further the spatial structure of these complex interaction patterns, we construct here in total 18 coupled climate networks consisting of two layers each, one layer representing sea surface temperature (SST) anomalies and the other geopotential height fields (HGT) at different pressure levels from 1000 to 10 mbar covering the entire troposphere as well as the lower stratosphere.

Our area of study covers the whole Northern Hemisphere north of 30°N so that the density of grid points in the considered climate data sets increases rapidly towards the poles and induces some bias in the unweighted network measures (Radebach et al. 2013; Tsonis et al. 2006). Therefore, the standard coupled network approach by Donges et al. (2011) is not sufficient in the present case. To overcome the problem associated with the heterogeneous spatial density of grid points interpreted as nodes of the climate network, Heitzig et al. (2012) introduced a novel set of network measures that takes into account the different sizes or weights of nodes in the network. By following an axiomatic approach, each *standard* (unweighted) network measure can be transformed into its weighted counterpart, the so-called *node splitting invariant* (n.s.i.) network measure. Corresponding n.s.i. measures have also been derived by Zemp et al. (2014) for edge-weighted and directed networks.

To quantify the topology of coupled climate networks, we rely in this work on the previously defined versions of local (i.e. node-wise) n.s.i. coupled network measures (Feng et al. 2012; Wiedermann et al. 2013) and additionally derive further weighted global network measures following the approach introduced by Heitzig et al. (2012). This allows us to assess and compare the macroscopic correlation structure in each of the 18 coupled climate networks.

We compare the results of MCA (e.g. Storch and Zwiers 2001), a well-established standard tool from statistical climatology, with the cross-degree density of nodes in the different subnetworks and confirm expected similarities between the two mea-

sures (Donges et al. 2015a). By utilizing network measures of higher order such as the n.s.i. local cross-clustering coefficient, we find that the statistical interrelation between ocean and atmosphere exhibits a hierarchical structure, in which individual parts or areas of the ocean surface correlate strongly with multiple statistically dissimilar parts of the atmosphere. Building upon previous studies by, e.g., Czaja and Frankignoul 1999; Frankignoul and Sennchael 2007, and Gastineau and Frankignoul 2015 we relate the observed hierarchy to dominant atmospheric patterns forcing the ocean on the time scales investigated in this study.

The remainder of this paper is organized as follows. Section 2 introduces the data sets and all methods, i.e., maximum covariance analysis and coupled climate network analysis, that are applied in this study. Section 3 presents all results of the analysis followed by conclusions and an outlook discussing future research tasks in Section 4.

2 Data & Methods

2.1 Data description

We construct coupled climate networks from two different climatic observables in order to investigate their interaction structure. One subnetwork is based on monthly anomalies of geopotential height (HGT) fields obtained from the ERA40 reanalysis project of the European Centre for Medium-Range Weather Forecast (Uppala et al. 2005). The data is given on a regular latitude/longitude grid with a spatial resolution of $\Delta\lambda = \Delta\phi = 2.5°$. In total, we investigate 18 layers of HGT fields. The corresponding pressure values at each isobaric surface as well as the average geopotential height are given in Tab. 1. The second subnetwork is constructed from the monthly averaged SST field (HadISST1) provided by the Met Office Hadley Centre (Rayner et al. 2003) with a resolution of $\Delta\lambda = \Delta\phi = 1°$. All grid points with corresponding time series containing missing values are removed from the data set as they represent areas which have been at least temporarily covered by sea-ice.

For our analysis we investigate all grid points north of $\lambda = 30°N$ excluding the North Pole itself. Both data sets are cropped in their temporal extent to cover the same time span from January 1958 to December 2001 and, hence, each time series consists of $T = 528$ temporal sampling points. We obtain a total number of $N_s = 6201$ grid points for the SST data and $N_i = 3456$ grid points for each isobaric surface i of HGT. For both data sets, we remove the annual cycle by subtracting the climatic mean for each month from each time series. Since we focus on the spatial structure of strong statistical interrelationships between ocean and atmosphere during boreal winter months (DJF), we use only the corresponding values which yields a length of each time series of $\tau = 132$ data points.

2.2 Maximum covariance analysis (MCA)

Consider two sets of time series $\{X_{s_n}(t)\}_{n=1}^{N_s}$ and $\{X_{i_m}(t)\}_{m=1}^{N_i}$ representing two different climatic fields, which in the scope of our application are the SST field (in what follows indicated by the index s) and one layer i of HGT (see also Tab. 1). Further

assume each individual time series in both fields to be normalized to zero mean and unit variance. The linear lag-zero cross-correlation matrix $\mathbf{C}_{si}$ with entries $C_{s_n i_m}$ is then defined as

$$C_{s_n i_m} = \frac{1}{\tau} \sum_{t=1}^{\tau} X_{s_n}(t) X_{i_m}(t), \tag{1}$$

where $n = 1, \ldots, N_s$, $m = 1, \ldots, N_i$ and τ denotes the total number of temporal sampling points in the two time series. Due to the heterogeneous spatial distribution of grid points in the present data sets all matrix entries $C_{s_n i_m}$ are additionally multiplied by the square roots of the cosine of latitudinal positions $\lambda_\bullet$ to ensure equal weighting. This then yields the weighted cross-correlation matrix $\mathbf{C}_{si}^w$ with entries

$$C_{s_n i_m}^w = \sqrt{\cos \lambda_{s_n} \cos \lambda_{i_m}} C_{s_n i_m}. \tag{2}$$

Analogously to empirical orthogonal function (EOF) analysis (e.g. Ghil et al. 2002; Hannachi et al. 2007), MCA identifies orthonormal pairs of coupled patterns $\vec{p}_s^{(m)} = (p_{s_1}^{(m)} \ldots p_{s_{N_s}}^{(m)})$ and $\vec{p}_i^{(m)} = (p_{i_1}^{(m)} \ldots p_{i_{N_i}}^{(m)})$ for $m = 1, \ldots, R$ (with R being the rank of $\mathbf{C}_{si}$) which explain as much as possible of the covariance between pairs of time series taken from the two different climatic fields (e.g. Bretherton et al. 1992; Storch and Zwiers 2001). The coupled patterns are obtained by solving the singular value problem of the weighted cross-covariance matrix,

$$\mathbf{C}_{si}^w \vec{p}_i^{(m)} = \sigma_m \vec{p}_s^{(m)}, \tag{3}$$
$$(\mathbf{C}_{is}^w)^{\mathbf{T}} \vec{p}_s^{(m)} = \sigma_m \vec{p}_i^{(m)}. \tag{4}$$

They are ordered according to their respective singular values σ_k with $\sigma_1 \geq \sigma_2 \geq \ldots \geq \sigma_R$. Hence, σ_1 denotes the largest among the R singular values that can be found to solve the above equations. Therefore, $\vec{p}_i^{(1)}$ and $\vec{p}_s^{(1)}$ are referred to as the *leading* coupled patterns representing the largest fraction of squared covariance between the two climatic fields given by σ_1^2.

2.3   Coupled climate network construction

In climate networks, each node represents a climatic time series and links indicate strong correlations between two series. Hence, the $N \times N$ ($N = N_s + N_i$) correlation matrix contains the pairwise linear statistical relationships between all time series considered for the network construction. Here, we independently construct coupled climate networks for all combinations of the SST field and each of the 18 isobaric surfaces of HGT, which shall be investigated separately and rely on the linear Pearson correlation coefficient as an appropriate measure of statistical association. Hence, the correlation matrix has the form

$$\mathbf{C} = \begin{pmatrix} \mathbf{C}_{ss} & \mathbf{C}_{si} \\ \mathbf{C}_{is} & \mathbf{C}_{ii} \end{pmatrix}. \tag{5}$$

The two block matrices $\mathbf{C}_{ss}$ ($N_s \times N_s$) and $\mathbf{C}_{ii}$ ($N_i \times N_i$) represent the (internal) correlation matrices of the SST and HGT fields, respectively, which consist of elements

$$C_{s_n s_m} = \frac{1}{\tau} \sum_{t=1}^{\tau} X_{s_n}(t) X_{s_m}(t), \quad n, m = 1, \ldots, N_s, \tag{6}$$

$$C_{i_n i_m} = \frac{1}{\tau} \sum_{t=1}^{\tau} X_{i_n}(t) X_{i_m}(t), \quad n, m = 1, \ldots, N_i. \tag{7}$$

The elements of $\mathbf{C}_{si} = \mathbf{C}_{is}^{\mathbf{T}}$ are derived according to Eq. (1). Note, that (in contrast to the computation of the leading coupled patterns) we construct the coupled climate networks from the *unweighted* correlation matrix $\mathbf{C}$, while the correction for the heterogeneous spatial distribution of nodes is implemented into the corresponding network measures (see Sec. 2.4).

From the correlation matrix $\mathbf{C}$ one generally derives the network's adjacency matrix $\mathbf{A}^+$ by setting a fixed threshold T such that only a certain fraction (i.e. the link density ρ) of strongest correlations is represented by links in the resulting climate network. For obtaining the adjacency matrix $\mathbf{A}^+$ of coupled climate networks, we refine this procedure by fixing a desired link density $\rho_s = \rho_i = 0.01$ for the structure of internal links within the two subnetworks representing SST and HGT fields, respectively. This means that only nodes with a correlation above the empirical 99th percentile of correlations between all time series within each field are connected. This condition then leads to internal correlation thresholds $T_s = 0.8101$ for the SST field and T_i for each isobaric surface of HGT (Tab. 1). Usually, the dynamics within the different climatic fields shows much higher cross-correlations than between them. We account for this fact by assuming the fraction of significant interactions between the climatic fields to be lower than those within them. Specifically, we request a cross-link density of $\rho_{si} = 0.005 < \rho_s = \rho_i$, which is lower than the internal ones, and derive a cross-threshold T_{si} for each layer of HGT individually (Fig. 1). All internal thresholds T_s and T_i are significantly larger than the obtained cross-thresholds T_{si}. Thus, setting a global link density or threshold would cause no or few cross-links to be present between the two fields or respective subnetworks. We further note that all links in each of the coupled climate networks represent correlations that are significant at least at the 95% confidence level of a standard t-test, where the degrees of freedom are determined by the total number of temporal sampling points τ in each of the time series (with $\tau = 132$ we thus obtain 130 degrees of freedom when neglecting the presence of serial correlations in the individual time series).

The different values of T_{si} already give an impression of the strength of correlation between the SST field and the different isobaric layers: low thresholds generally indicate weaker correlations while high thresholds imply stronger similarity between both fields. Further we note that the resulting cross-thresholds vary smoothly with

the choice of cross-link density (Fig. 1) and we thus consider the construction mechanism to be sufficiently insensitive to the actual choice of cross-link density.

Using the different thresholds introduced above, we obtain the coupled climate network's adjacency matrix by individually thresholding the absolute correlation values between and within both fields as

$$\mathbf{A}^+ = \begin{pmatrix} \Theta(|\mathbf{C}_{ss}| - T_s) & \Theta(|\mathbf{C}_{si}| - T_{si}) \\ \Theta(|\mathbf{C}_{is}| - T_{si}) & \Theta(|\mathbf{C}_{ii}| - T_i) \end{pmatrix},$$

where $\Theta(\cdot)$ denotes the Heaviside function. Note that in most recent studies on climate networks self-loops (resulting in a non-vanishing trace of the adjacency matrix) have been excluded. In this case the adjacency matrix is usually denoted as $\mathbf{A}$. Since we aim to apply node splitting invariant network measures (see below) to quantify the network's topology we specifically demand each node to be connected with itself. The resulting matrix $\mathbf{A}^+$ is referred to as the *extended* adjacency matrix (Heitzig et al. 2012). Further note, that the usage of the term *coupled* in *coupled climate networks* does not imply the notion of any directionality or causal influence between the two fields under study. It is simply meant to indicate the fact that the network under study is composed of more than a single climatic field.

2.4   Coupled network characteristics

The local (point-wise) and global structure of a climate network can be quantified by a variety of network measures (Albert and Barabási 2002; Donges et al. 2009a; Newman 2003), which can generally be interpreted as specific operations on the adjacency matrix. The climate networks in this study are constructed from climate data sets where the density of grid points and, hence, the density of nodes in the network, rapidly increases towards the North pole. In order to avoid a bias in the evaluation of the climate network's structure, we account for this effect by relying on node-weighted network measures and value nodes with a gradually decreasing weight as one moves from the equator towards the pole. To quantify the correlation structure between ocean and atmosphere at each node we focus on two previously defined node weighted local network measures, the n.s.i cross-degree (Feng et al. 2012) and the n.s.i. local cross-clustering coefficient (Wiedermann et al. 2013). In addition, we utilize the construction mechanism introduced by Heitzig et al. (2012) to convert global interacting network measures (Donges et al. 2011) into their weighted counterparts.

2.4.1   Preliminaries

Consider a coupled climate network $G = (V, E)$ with a set of nodes V, links E and the number of nodes $N = |V|$. Following the general naming convention in the climate network framework we identify every node $v \in V$ with a natural number $p = 1, \ldots, N$, such that p serves as the label of the node as well as an index to corresponding network characteristics. The network G is represented by its adjacency matrix $\mathbf{A}$ with $A_{pq} = 1$ if $(p, q) \in E$, $A_{pq} = 0$ if $(p, q) \notin E$. In this study, each coupled climate network is composed of two subnetworks, $G_s = (V_s, E_{ss})$ representing

the ocean and $G_i = (V_i, E_{ii})$ representing a specific atmospheric layer. The set of nodes V divides into subsets V_s and V_i such that each node belongs to exactly one subnetwork (i.e. $V = V_s \cup V_i$ and $V_s \cap V_i = \emptyset$). Likewise, the set of links E splits into internal link sets E_{ss} and E_{ii} (connecting nodes within a subnetwork) and cross-link sets E_{si} connecting nodes $v \in V_s$ with nodes $q \in V_i$ in the subnetworks G_s and G_i, respectively (Donges et al. 2011).

In the present case (as for all regularly gridded climate data sets) the share on the entire area of the surface that is represented by each node is governed by its latitudinal position λ_v on the grid. Following Tsonis et al. (2006), we therefore assign to each node v in the climate network a weight

$$w_v = \cos \lambda_v. \qquad (8)$$

Note that, by following this convention the climate networks' node weights w_v exhibit the same dimension as the weights of the cross-covariance matrix in Eq. (2).

Heitzig et al. (2012) introduced a novel set of *node splitting invariant* (n.s.i.) network measures to quantify the topology of a climate network with such a heterogeneous spatial node density for the case of a single-layer network and, hence, only one climate variable under study. In fact, the n.s.i. network measures are not restricted to climate networks but can be utilized to study any type of single-layer complex network where nodes represent entities of different weights. Heitzig et al. (2012) further showed that each complex network measure can be transformed into its weighted counterpart by using a four-step construction mechanism:

(a) Sum up weights w_v whenever the unweighted measure counts nodes.

(b) Treat every node $v \in V$ as connected with itself.

(c) Allow equality in summations over indices v and q wherever the original measure involves a sum over distinct nodes v and q.

(d) "Plug in" n.s.i. versions of measures wherever they are used in the definition of other measures.

From the definition of the adjacency matrix $\mathbf{A}^+$ in Eq. (8) we note that step (b) of the above scheme is in our case already fulfilled. Wiedermann et al. (2013) and Zemp et al. (2014) recently utilized the proposed scheme to convert local interacting network measures as well as measures for directed networks into their weighted counterparts. Here, we additionally derive n.s.i. versions of some global cross-network measures that were introduced by Donges et al. (2011).

2.4.2 Local measures

For quantifying local cross-network interactions in coupled climate networks we rely on two measures, n.s.i. cross-degree k_v^{j*} and n.s.i. local cross-clustering coefficient $\mathcal{C}_v^{j*}$, that were introduced by Wiedermann et al. (2013) and (for the case of the n.s.i. cross-degree) by Feng et al. (2012). These two measures are defined as

$$k_v^{j*} = \sum_{q \in V_j} w_q A_{vq}^+, \tag{9}$$

$$\mathcal{C}_v^{j*} = \frac{1}{\left(k_v^{j*}\right)^2} \sum_{p,q \in V_j} A_{vp}^+ A_{pq}^+ A_{qv}^+ w_q w_p \in [0,1]. \tag{10}$$

In contrast to the unweighted cross-degree

$$k_v^j = \sum_{q \in V_j} A_{vq}^+ \tag{11}$$

which simply counts nodes $q \in V_j$ that are connected with $v \in V_i$, k_v^{j*} is proportional to the share on the considered overall ice-free ocean or isobaric surface area, respectively, that is connected with nodes $v \in V_j$ in the other subnetwork. It therefore gives a notion of how similar the dynamics at a node $v \in V_i$ is to that of the other climate variable observed at all available grid points.

Similar to k_v^{j*}, $\mathcal{C}_v^{j*}$ no longer relies on the counting of distinct fully connected node triples in the network (as for the classical local clustering coefficient (Newman 2003)) but on the weighted sum of occurrences of triples of connected areas within the two subnetworks. It gives the probability that an area represented by a node $v \in V_i$ is connected with two mutually connected and, hence, dynamically similar, areas in the opposite subnetwork. In this spirit, $\mathcal{C}_v^{j*}$ estimates how likely areas in two different climatic fields or subsystems form clusters of statistical equivalence between them. A local accumulation of such connected triples represents clusters of closely connected nodes and, in the spirit of climate networks, strongly correlated regions.

In order to make the n.s.i. cross-degree k_v^{j*} comparable between the two subnetworks, we normalize it by the maximum possible weight that nodes $v \in V_i$ can be connected with,

$$\kappa_v^{j*} = \frac{\sum_{q \in V_j} w_q A_{vq}^+}{W_j} \in [0,1]. \tag{12}$$

In the spirit of earlier work by Donges et al. (2012) and Donner et al. (2010), we refer to this quantity as the *n.s.i. cross-degree density*. Here, $W_j = \sum_{q \in V_j} w_q$ denotes the total weight of all nodes $q \in V_j$. For the case of a single-layer network, a measure similar to the n.s.i. cross-degree density has been introduced by Tsonis et al. (2006) in terms of the *area weighted connectivity*, which quantities the share on the subdomain of interest represented by the entire network G that is connected with any nodes $v \in V$.

Generally, Wiedermann et al. (2013) and Zemp et al. (2014) showed that the weighted local cross-network measures improve the representation of a network's topology with inhomogeneous node density within the domain of interest in comparison with its unweighted counterparts.

Donges et al. (2015a) showed that for the unweighted case cross-degree and leading coupled patterns display strong similarity if the first coupled patterns explain a high fraction of the system's covariance. A similar assessment can be made for the similarity between the leading coupled patterns obtained from a weighted cross-covariance matrix and the n.s.i. cross-degree (see supporting information).

2.4.3 Global measures

In addition to local (per node) network measures we also aim to characterize the macroscopic interaction structure of each pair of coupled climate networks by means of global network properties. For coupled climate networks a variety of unweighted measures have been proposed by Donges et al. (2011). Here, we utilize the construction mechanism by Heitzig et al. (2012) to convert two of them into their weighted counterparts as well.

N.s.i. global cross-clustering coefficient. The global cross-clustering coefficient $\mathcal{C}_{ij}$ of a subnetwork G_i gives the probability that for a randomly chosen node $v \in V_i$ one finds neighbors $p, q \in V_j$ that are mutually linked. It is defined as the arithmetic mean of all local cross-clustering coefficients $\mathcal{C}_v^j$,

$$\mathcal{C}_{ij} = \frac{1}{N_i} \sum_{v \in V_i} \mathcal{C}_v^j. \tag{13}$$

This measure can be converted into its n.s.i. counterpart by calculating the weighted mean of all values of $\mathcal{C}_v^{j*}$,

$$\mathcal{C}_{ij}^* = \frac{1}{W_i} \sum_{v \in V_i} w_v \mathcal{C}_v^{j*}. \tag{14}$$

Again, analogously to the interpretation of the local n.s.i. measures, $\mathcal{C}_{ij}^*$ no longer only measures pure node-wise triangular structures but takes into account the share on the Earth's surface areas involved in the formation of triangular structures. Generally, large values of $\mathcal{C}_{ij}^*$ (which are induced by a dominance of connected triples between the two subnetworks under consideration) indicate strong transitivity in the underlying correlation structure.

N.s.i. cross-transitivity. The cross-transitivity $\mathcal{T}_{ij}$ gives the probability that two randomly drawn nodes $p, q \in V_j$ are connected if they have a common neighbor $v \in V_i$. It is given as

$$\mathcal{T}_{ij} = \frac{\sum_{v \in V_i} \sum_{p \neq q \in V_j} A_{vp} A_{pq} A_{qv}}{\sum_{v \in V_i} \sum_{p \neq q \in V_j} A_{vp} A_{qv}}. \tag{15}$$

Like $\mathcal{C}_{ij}$, the cross-transitivity is a measure of organization with respect to the cross-correlation structure in a coupled network (Donges et al. 2011). However, in contrast

to $\mathcal{C}_{ij}$, $\mathcal{T}_{ij}$ takes into account the increasing influence of nodes with high cross-degree and weighs them more heavily than nodes with low cross-degree. More importantly it ignores nodes with no links into the opposite layer, since these nodes display a zero cross-degree. The node-weighted variant of $\mathcal{T}_{ij}$ can be written as

$$\mathcal{T}_{ij}^* = \frac{\sum_{v \in V_i} \sum_{p,q \in V_j} w_v A_{vp}^+ w_p A_{pq}^+ w_q A_{qv}^+}{\sum_{v \in V_i} \sum_{p,q \in V_j} w_v A_{vp}^+ w_p w_q A_{qv}^+} = \frac{\sum_{v \in V_i} w_v (k_v^{j*})^2 \mathcal{C}_v^{j*}}{\sum_{v \in V_i} w_v (k_v^{j*})^2}. \tag{16}$$

We note that both $\mathcal{C}_{ij}^*$ and $\mathcal{T}_{ij}^*$ similarly evaluate the transitivity of correlations between the two climatic variables under study and, hence, quantify a similar network property. They are derived, however, in a disjoint manner. One measure, $\mathcal{C}_{ij}^*$ is computed as the weighted average taken over $\mathcal{C}_v^{j*}$. In contrast, despite suggestions by Radebach et al. (2013) to decompose the global transitivity into local contributions, the n.s.i. cross-transitivity $\mathcal{T}_{ij}^*$ is defined solely as a global network measure with no direct local counterpart. It is important to note that n.s.i. cross-transitivity and n.s.i. global cross-clustering coefficient are commonly asymmetric in the sense that $\mathcal{T}_{ij}^* \neq \mathcal{T}_{ji}^*$ and $\mathcal{C}_{ij}^* \neq \mathcal{C}_{ji}^*$.

3 Results

3.1 Maximum covariance analysis (MCA)

We start our analysis by computing the leading coupled patterns between the SST field and the 18 HGT layers for boreal winter (DJF). Figure 2 displays the results for three representative layers of HGT at 50 mbar, 100 mbar and 500 mbar.

By applying MCA, we detect coherent large-scale patterns of winter SST, which co-vary with the winter atmospheric circulation structures instantaneously. The leading MCA patterns explain rather large amounts of 42%, 63% and 70% (for the 500, 100 and 50 mbar pressure level, respectively) of the squared covariance. At all levels, the leading MCA mode displays significant SST anomalies over the North Pacific with maximum values along the sub-Arctic front near 40°N, and anomalies of the opposite sign along the western coast of North America (Fig. 2A,C,E) (An and Wang 2005; Frankignoul and Sennchael 2007). Over the North Atlantic, a dipole structure is seen between the northern part of the Gulf Stream and the Atlantic Ocean south of Greenland including parts of the Davis Strait and the North Atlantic current. This pattern resembles the first SST EOF for the Northern Hemisphere during boreal winter (not shown).

This general SST pattern is co-varying with a pressure anomaly pattern showing a hemispheric annular-like structure in the upper troposphere and lower stratosphere (Fig. 2B,D). In the mid-troposphere (Fig. 2F), this pattern displays wave-like deviations from the annular structure, which show distinct similarities with the wave-train structure of the Pacific North American (PNA) pattern. Therefore, the leading MCA mode relates negative SST anomalies along the sub-Arctic front with a positive PNA phase.

The second MCA mode (not shown, explaining 13%, 17% and 21% of the squared covariance fraction for the 500, 100 and 50 mbar pressure level, respectively) displays the strongest SST anomalies over the North Atlantic. Over that region, the SST pattern resembles the northern part of the North Atlantic SST tripole pattern which is related with the North Atlantic Oscillation (NAO) (e.g. Czaja and Frankignoul 1999; Czaja and Frankignoul 2002; Gastineau and Frankignoul 2015). Accordingly, the co-varying atmospheric pattern in the middle troposphere shows the cold ocean/warm land (COWL) pattern (introduced by Wallace et al. (1996)) including a NAO-like dipole over the North Atlantic. At higher levels, the co-varying atmospheric patterns display a pronounced wave number-2 pattern.

By applying lagged MCA between SST and mid-tropospheric circulation fields, several studies for the North Atlantic and the North Pacific have shown that the squared covariance fraction is strongest and most significant at lags of 0 and 1 month during late fall and winter (e.g. Czaja and Frankignoul 1999; Frankignoul and Sennchael 2007; Gastineau and Frankignoul 2015; Liu et al. 2006; Wen et al. 2005). This points to the forcing of the SST by the dominant atmospheric pattern, which is the PNA pattern over the Pacific-North American sector (e.g. Frankignoul and Sennchael 2007) and the North Atlantic Oscillation (NAO) over the North Atlantic-European region (Czaja and Frankignoul 1999; Gastineau and Frankignoul 2015). On the other hand, results of lagged MCA analyses with the ocean leading by 1 to 4 months in Frankignoul and Sennchael (2007) and Gastineau and Frankignoul (2015) suggest that the SST anomalies have a substantial influence on the large-scale atmospheric circulation at these time-scales.

3.2   Local coupled network measures

In order to first demonstrate the general consistency of coupled climate network analysis in comparison with MCA, we continue by generating coupled climate networks between the SST field and the three previously considered layers of geopotential height (500 mbar, 100 mbar, 50 mbar). The n.s.i. cross-degree densities κ_v^{i*} and κ_v^{s*} are expected to display similar spatial structures as the corresponding leading coupled patterns (Donges et al. 2015a) since the latter explain a high share of the cross-covariance between both fields (see supporting information).

As demonstrated in Fig. 3, the results for κ_v^{s*} and κ_v^{i*} indeed match well the results obtained from the MCA when comparing the locations of maximum values in the coupled network's n.s.i. cross-degree densities to those of maximum or minimum values in the leading mode of the MCA. Note, that the n.s.i. cross-degree densities κ_v^{s*} and κ_v^{i*} take, per definition, only positive values, while coupled patterns display both, positive and negative values. Hence, κ_v^{s*} and κ_v^{s*} only reproduce structures that coincide with the absolute values of the leading coupled patterns. However, as only a certain percentage of squared covariance is explained by the leading coupled patterns, we also note differences between the patterns revealed by the two methods. In particular, the negative center of action around the North Pole that is detected by MCA is only weakly present in the cross-degree density fields κ_v^{s*} for the 50 and 100 mbar HGT fields (compare Fig. 2B,D with Fig. 3B,D). For the ocean, preferably the marked structures in the leading coupled patterns in both the Atlantic and the

Pacific are well recovered by the cross-degree density κ_v^{i*} while some of the weaker structures, e.g. in the Black Sea, are missing.

Network analysis, however, allows us to undertake a further in-depth analysis of the correlation structure between the different layers beyond the information provided by MCA. The n.s.i. local cross-clustering coefficients $\mathcal{C}_v^{i*}$ and $\mathcal{C}_v^{s*}$ (Eq. (10)) give the probabilities that the dynamics at a grid point in, e.g., the SST field is similar to that at two grid points in the HGT field, which behave themselves statistically similar. Note that in the scope of this work we do not account for any possible effects induced by a common external forcing of the fields, which might artificially induce correlations and, hence, cause the presence of spurious links between nodes or triples of nodes. We also do not account for indirect (partial) correlations or common driver effects within each of the fields when constructing the coupled climate networks. Conditioning out these possible influences by means of information theoretic approaches (Runge et al. 2012; Runge et al. 2014) and causal effect networks (Kretschmer et al. 2016; Runge et al. 2015) thus remains as a subject of future research.

Figure 4 presents the results for the n.s.i. local cross-clustering coefficients $\mathcal{C}_v^{i*}$ for nodes in the SST field (Fig. 4A,C,E) and $\mathcal{C}_v^{s*}$ for nodes in the HGT fields (Fig. 4B,D,F). Most nodes in the SST field tend to display a low n.s.i. local cross-clustering coefficient $\mathcal{C}_v^{i*} < 0.2$ (Fig. 4A,C,E) and, thus, preferentially correlate with nodes in the HGT fields that are mutually dissimilar and therefore disconnected (Fig. 5). In contrast, many nodes in the HGT fields exhibit a comparatively high or intermediate n.s.i. local cross-clustering coefficient $0.4 < \mathcal{C}_v^{s*} < 1$ (for one of the most prominent examples compare nodes located at or above the Pacific in Fig, 4B,D). Quantitatively, for the combination of the SST and the 500 mbar HGT field we find an n.s.i. global cross-clustering coefficient (Eq. (14)) of $\mathcal{C}_{si}^* = 0.16$ for SST nodes and $\mathcal{C}_{is}^* = 0.28$ for 500 mbar HGT nodes. Ignoring those nodes in the averaging that display zero n.s.i. cross-degree density we obtain values of $\mathcal{C}_{si}^{*\prime} = 0.42$ and $\mathcal{C}_{is}^{*\prime} = 0.52$ (note that this definition is different from the one presented in Eq. (14) as we specifically exclude the contribution of nodes with no links to the opposite subnetwork). The n.s.i. cross-transitivity (Eq. (16)) which weighs nodes according to their n.s.i. cross-degree density gives values of $\mathcal{T}_{si}^* = 0.2$ and $\mathcal{T}_{is}^* = 0.25$ for nodes in ocean and atmosphere, respectively. For all three measures, the values computed for the atmospheric subnetwork exceed those for the ocean and thus consistently imply that nodes in the ocean are less likely to connect with mutually connected nodes in the atmosphere than vice versa.

To further quantify the asymmetries in the correlation structure between ocean and atmosphere, we investigate for each node with a given n.s.i. cross-degree density its corresponding n.s.i. local cross-clustering coefficient in a coupled climate network composed of the SST and 500 mbar HGT fields (Fig. 6). This layer is chosen as it provides a good indication of the atmospheric circulation over the area of study (Gastineau and Frankignoul 2015; Kushnir et al. 2002). Furthermore, it displays among the highest values of T_{si} according to Fig. 1, which has similarly been described as a *strong statistical signal* by Frankignoul and Sennchael (2007).

For nodes in the SST field (Fig. 6A), we find that $\mathcal{C}_v^{i*}(\kappa_v^{i*})$ tends to follow a power-law, $\mathcal{C}_v^{i*} \sim (\kappa_v^{i*})^{-\alpha}$, which indicates a hierarchical network structure (Ravasz

et al. 2002; Ravasz and Barabási 2003) which, in contrast, is absent for nodes in the HGT field (Fig. 6B). Here, the term *hierarchical* implies that nodes in the SST field strongly correlate with disconnected clusters of statistically similar nodes in the HGT field as depicted in Fig. 5. This deduction is further supported by the fact that for the HGT field, the distribution of combinations of $\mathcal{C}_v^{s*}$ and κ_v^{s*} is more widely spread and $\mathcal{C}_v^{s*}$ generally takes higher values than $\mathcal{C}_v^{i*}$. This implies that nodes in the HGT field show a stronger tendency to correlate with mutually connected nodes in the SST field, which can be assumed to display a strong statistical similarity among themselves (Molkenthin et al. 2014; Tupikina et al. 2014). To test for the robustness of our results we have carried out the same analysis as presented in Fig. 6 for internal link densities of $\rho_{ss} = \rho_{ii} = 0.02$ and $\rho_{ss} = \rho_{ii} = 0.05$, and corresponding cross-link densities $\rho_{si} = 0.01$ and $\rho_{si} = 0.025$ (see Figs. 1 and 2 in the supporting information). Even though the power-law exponent α slightly decreases towards zero with increasing link densities, we find that the qualitative findings remain unchanged. We thus consider our analysis to be sufficiently robust with respect to the actual choice of link densities.

As a remark, we note a general tendency of nodes at the boundaries of a cluster that links with the opposite field to display comparatively low values of n.s.i. cross-degree density and increased values of n.s.i. local cross-clustering coefficient (Fig. 3 and Fig. 4). In contrast, nodes located towards the center of these clusters display increased n.s.i. cross-degree density, which is in general to be expected from the continuity of the underlying system. However, in that case we also note tendencies for decreased values of n.s.i. local cross-clustering coefficients. This observation is a result of the fact that especially those nodes with only one link to the opposite field show by definition the highest value of the n.s.i. local cross-clustering coefficient, $\mathcal{C}_v^{j*} = 1$. With increasing n.s.i. cross-degree density this measure converges to a more reasonable estimate of a node's tendency to cluster.

One way to address this issue in the future would be to subtract the squared sum of weights w_v of all neighbors of the considered node from the numerator in Eq. (10). Such procedure would, however, introduce a non-standard network measure whose properties should be assessed thoroughly in future research before applying it to climatic studies. To this end, we acknowledge that the concerned nodes do not play a crucial role for the propositions put forward in this section, since they (i) are ultimately dealt with by the assessment of n.s.i. cross-transitivity which weighs those corresponding nodes much lower than those with a high n.s.i. cross-degree density and (ii) only manifest in the very upper left corners of Fig. 6A,B. In that case they do not contribute significantly to the observed relationship between n.s.i. cross-degree density and n.s.i. local cross-clustering coefficient and have no further impact on the qualitative statements put forward above.

Following upon the quantitatively observed hierarchy, Fig. 7 allows for a visual inspection of some illustrative parts of the corresponding network structure. In particular, we display for two selected patches of nodes in the SST field that show high values of κ_v^{i*} with the HGT field (blue and orange shaded polygons in Fig. 7A) their corresponding neighboring nodes in the HGT field as well as all links between those nodes (respective blue and orange scatter in Fig. 7A). While ignoring very small clusters we find in total four (three) substantial mutually disconnected patches

of nodes in the HGT field that correlate with the respective ocean patches. Vice versa, by selecting the resulting two largest patches of nodes in the HGT field above both oceans (blue and orange shaded polygons in Fig. 7B) we find that each of the patches only correlates with two disconnected patches of nodes in the SST field that are of a relevant spatial extent to have an effect on the estimation of $\mathcal{C}_v^{s*}$. Thus, the resulting n.s.i. cross-clustering coefficient $\mathcal{C}_v^{i*}$ for nodes in the ocean exceed $\mathcal{C}_v^{s*}$ for nodes in the atmosphere as the ocean correlates with more mutually disconnected clusters of nodes than vice versa.

Comparing the observed node patches in the HGT field with atmospheric patterns of large-scale variability patterns (Handorf and Dethloff 2012), we relate the two atmospheric clusters in the HGT field that are located above the Atlantic (blue scatter in Fig. 7A) with the NAO. Correspondingly, the three patches located above the Pacific (orange scatter in Fig. 7A) coincide well with the spatial signature of the PNA pattern. Taking into account past studies that applied lagged correlation analysis we note that on the time scales considered in this study the atmosphere serves as a driving force of the ocean along the spatial domain that is of interest here (e.g. Czaja and Frankignoul 1999; Frankignoul and Sennchael 2007; Gastineau and Frankignoul 2015). Thus, the hierarchical network structure might on the one hand be a result of the aforementioned atmospheric forcing to the ocean. On the other hand, with reference to Fig. 7, the framework of coupled climate networks and the methodology put forward in this work serve to resolve the corresponding induced correlation structure between the two climatic subsystems in a spatially explicit way, such that it enables to specifically detect forcing and forced areas in atmosphere and ocean, respectively.

Choosing different HGT layers up to 200 mbar yield similar results (not shown). This aligns well with previous results by Czaja and Frankignoul (1999) and Frankignoul and Sennchael (2007) who observed comparable spatial statistical patterns at each tropospheric level. Thus, the observed hierarchy seems to be a generic property of the troposphere. Following the above lines of thought, future work should investigate coupled climate networks constructed from lagged cross-correlations to investigate whether the observed structures are indeed a result of short-term atmosphere-to-ocean forcing. Such procedure would, however, require the derivation of novel directed interacting network measures, which in turn would provide a valuable extension to the framework of climate network analysis.

3.3   Global measures

So far we have focused our study on three atmospheric layers, namely the 50 mbar, 100 mbar and 500 mbar HGT field. Specifically for the latter case, we have carried out a further in-depth analysis of the observed hierarchical structures by means of assessing the power-law relationship between κ_v^{i*} and $\mathcal{C}_v^{i*}$ as well as investigating the distinct spatial distribution of nodes and links in ocean and atmosphere that obey the observed hierarchical organization (Fig. 7). To show that these structures are (i) not only present for the 500 mbar field and (ii) their observations are robust with respect to the choice of link densities we investigate global network characteristics that provide a macroscopic description of the observed network structures.

Specifically, we study the n.s.i. cross-transitivity $\mathcal{T}_{si}^*$ computed over nodes in the SST field and $\mathcal{T}_{is}^*$ computed over nodes in each of the HGT fields according to Eq. (16) together with the n.s.i. global cross-clustering coefficients $\mathcal{C}_{si}^*$ and $\mathcal{C}_{is}^*$, respectively (Eq. (14)). Note again that the latter are defined as the weighted means of their local counterparts that are presented in Fig. 4, where nodes with no links to the opposite field are weighted in the same fashion as those with adjacent cross-links. In contrast, the n.s.i. cross-transitivity assigns nodes a weight corresponding to their n.s.i. cross-degree (which for the case of no adjacent cross-links takes a value of zero) and, thus, excludes them from the averaging.

The corresponding results are summarized in Fig. 8. We find that both $\mathcal{T}_{si}^*$ and $\mathcal{C}_{si}^*$ show their maximum values at around 10 km altitude (250 mbar) (Figs. 8A and 8B). For the same quantities, distinct minima at 850 mbar (1.4 km) coincide with the transition from the atmospheric boundary layer to the lower troposphere as also found in Donges et al. (2011). For all layers above 100 mbar, $\mathcal{T}_{si}^*$ remains almost constant at low values. Hence, $\mathcal{T}_{si}^*$ and $\mathcal{C}_{si}^*$ seem to naturally discriminate between three different atmospheric layers: below 850 mbar (atmospheric boundary layer), between 850 mbar and 100 mbar (free troposphere) and above 100 mbar (lower stratosphere).

For the global measures computed over all nodes in the HGT field, we find that the n.s.i. cross-transitivity $\mathcal{T}_{is}^*$ shows almost constant values for all layers below 200 mbar and, hence, again separates well the dynamics within the troposphere from that inside the stratosphere (Fig. 8C). For all layers above 200 mbar $\mathcal{T}_{is}^*$ becomes almost independent of the cross-link density ρ_{si} that is fixed when constructing the network. The same property also holds for the n.s.i. global cross-clustering coefficient $\mathcal{C}_{is}^*$ computed over all nodes in the different HGT fields (Fig. 8D).

In agreement with the local measures discussed in Sec. 3.2 we find that n.s.i. cross-transitivity and n.s.i. global cross-clustering coefficients are in most cases larger for nodes in the HGT fields than for nodes in the SST field (compare Fig. 8A with Fig. 8C and Fig. 8B with Fig. 8D). As for the n.s.i. local cross-clustering coefficients this indicates again the hierarchical network structure, i.e., a tendency for nodes in the HGT field to form triangular structures with nodes in the SST field, that is present across all atmospheric layers ranging from the troposphere to the lower stratosphere. The detailed structure of this hierarchy, however, seems to vary with the different atmospheric layers under study.

This observation further holds not only for the case of $\rho_{si} = 0.005$ that was used in the previous sections but also for larger values that are chosen from a reasonable range (Fig. 8). Thus, we consider our results to be sufficiently robust with respect to the choice of the networks' link densities.

In general, we observe that the quantitative and qualitative properties of the n.s.i. cross-transitivity and n.s.i. global cross-clustering coefficients vary with the different atmospheric layers. Hence, these global characteristics may serve to inter-compare and distinguish between different correlation structures in a coupled climate network. An in-depth analysis of the mechanisms that cause the occurrence of this behavior in our specific application remains as a subject of future research.

4   Conclusions & Outlook

We have carried out a detailed analysis of the correlation structure between atmospheric and ocean dynamics in the Northern Hemisphere extratropics from the viewpoint of coupled climate networks. Comparison between the n.s.i. cross-degree density (measuring the weighted share of significant correlations between grid points in different layers) and the leading mode of the maximum covariance analysis (MCA) reveals an expected high congruence between both methods for the considered data sets. However, coupled network analysis, and particularly the investigation of higher-order network parameters, allows us to further disentangle the underlying correlation structure. The (average) n.s.i. cross-degree density in combination with the (average) n.s.i. local cross-clustering coefficient provides additional insights on areas in the ocean and the atmosphere that show strong mutual correlations as well as localized versus delocalized correlation structures with the respective opposite field. In the SST field nodes tend to correlate with multiple mutually unconnected groups of similar nodes within the respective HGT fields. From investigating the interdependency between n.s.i. cross-degree density and n.s.i. local cross-clustering coefficient, we have found that the correlations between the ocean and the atmosphere exhibit a hierarchical structure in the sense of a power-law relationship between both properties. A visual inspection of the coupled climate network for the case of the 500 mbar HGT field reveals that the observed structure could be related with a forcing of the ocean by the dominant atmospheric patterns above the Atlantic and the Pacific. Ultimately, global network characteristics further support the results obtained from their local correspondents by showing that the observed structure is valid for large parts of the atmosphere ranging from the troposphere to the lower stratosphere.

In order to discriminate between the internal variability of the fields under study and possible influences of an external forcing, future work should analyze ensemble simulations of general circulation models to rule out common driver effects or assess the likelihood of their influence on the observed structures. In order to investigate the influence of spatio-temporal auto-correlation on the outcome of the present analysis the network could be alternatively constructed by estimating pairwise thresholds from surrogate data as proposed by Paluš et al. 2011. This approach would, however, break the comparability of the network approach with that of maximum covariance analysis, such that a different way of validating and comparing the results must be found. Comparability could be achieved by assessing synthetic model data, e.g., created from an auto-regressive process based on principal components of the data sets under study, and the application of both, MCA and network analysis. In addition to probable influences of auto-correlation such a process would allow to assess the influence of different time scales in ocean and atmosphere on the involved network characteristics.

Besides all possible future lines of work with respect to the climatic side of this work, from a network-theoretic point of view it is worthwhile to construct climate networks using more advanced causal estimators (e.g. Runge et al. 2012; Runge et al. 2014; Runge et al. 2015) to disentangle direct from indirect or externally and internally forced correlations.

To this end, our analysis has only been performed for the pairwise correlation

between one atmospheric layer and the ocean. Future studies should further explore the possibility to refine the proposed methods to also quantify interactions in a climate network existing of more than two subnetworks. Specifically, when studying coupled climate networks in the Northern Hemisphere, one should also consider Arctic sea ice as an additional observable in the network construction. Its dynamics has already been discovered as an influencing factor on atmospheric teleconnections and the dynamics of land snow cover in the Northern Hemisphere (Handorf et al. 2015). The study of coupled climate networks can help here to further disentangle and quantify possible changes in correlations between ocean and atmosphere over the course of the past decades that may have been induced by processes related to the Arctic amplification (Serreze and Francis 2006). Moreover, it is of great interest to apply our methods not only to coupled networks composed of different climatic fields (as presented in this work), but also to networks constructed from just one single climatic field that divides into dynamically distinct areas (Hlinka et al. 2014) or communities (Steinhaeuser et al. 2011; Tsonis et al. 2010). The framework presented in this work could then be utilized to study and quantify correlations between these detected or defined regions on or parallel to the Earth's surface. This would allow for a detailed investigation of correlation structures between different climatic subsystems such as, for example, the Indian Summer Monsoon and the El Niño Southern Oscillation.

Finally, it remains to remark that the weighted network measures presented in this work provide a general framework which can be applied to quantify interdependencies in complex networks representing subjects of study taken from many other fields beyond climatology.

Acknowledgements

References

Albert, R. and A.-L. Barabási (2002). "Statistical mechanics of complex networks". In: *Reviews of Modern Physics* 74.1, pp. 47–97. DOI: `10.1103/RevModPhys.74.47`.

An, S.-I. and B. Wang (Mar. 2005). "The Forced and Intrinsic Low-Frequency Modes in the North Pacific". In: *Journal of Climate* 18.6, pp. 876–885. DOI: `10.1175/JCLI-3298.1`.

Boccaletti, S., G. Bianconi, R. Criado, C. I. del Genio, J. Gómez-Gardeñes, M. Romance, I. Sendiña-Nadal, Z. Wang, and M. Zanin (Nov. 2014). "The structure and dynamics of multilayer networks". In: *Physics Reports* 544.1, pp. 1–122. DOI: 10.1016/j.physrep.2014.07.001.

Boers, N., B. Bookhagen, H. M. J. Barbosa, N. Marwan, J. Kurths, and J. A. Marengo (Oct. 2014a). "Prediction of extreme floods in the eastern Central Andes based on a complex networks approach". In: *Nature Communications* 5.5199. DOI: 10.1038/ncomms6199.

Boers, N., B. Bookhagen, N. Marwan, J. Kurths, and J. Marengo (Aug. 2013). "Complex networks identify spatial patterns of extreme rainfall events of the South American Monsoon System". In: *Geophysical Research Letters* 40.16, pp. 4386–4392. DOI: 10.1002/grl.50681.

Boers, N., R. V. Donner, B. Bookhagen, and J. Kurths (Aug. 2014b). "Complex network analysis helps to identify impacts of the El Niño Southern Oscillation on moisture divergence in South America". In: *Climate Dynamics*. DOI: 10.1007/s00382-014-2265-7.

Bretherton, C. S., C. Smith, and J. M. Wallace (June 1992). "An Intercomparison of Methods for Finding Coupled Patterns in Climate Data". In: *Journal of Climate* 5.6, pp. 541–560. DOI: 10.1175/1520-0442(1992)005<0541:AIOMFF>2.0.CO;2.

Buldyrev, S. V., R. Parshani, G. Paul, H. E. Stanley, and S. Havlin (Apr. 2010). "Catastrophic cascade of failures in interdependent networks". In: *Nature* 464.7291, pp. 1025–1028. DOI: 10.1038/nature08932.

Czaja, A. and C. Frankignoul (Oct. 1999). "Influence of the North Atlantic SST on the atmospheric circulation". In: *Geophysical Research Letters* 26.19, pp. 2969–2972. DOI: 10.1029/1999GL900613.

Czaja, A. and C. Frankignoul (Mar. 2002). "Observed Impact of Atlantic SST Anomalies on the North Atlantic Oscillation". In: *Journal of Climate* 15.6, pp. 606–623. DOI: 10.1175/1520-0442(2002)015<0606:OIOASA>2.0.CO;2.

Donges, J. F., Y. Zou, N. Marwan, and J. Kurths (July 2009a). "Complex networks in climate dynamics". In: *The European Physical Journal Special Topics* 174.1, pp. 157–179. DOI: 10.1140/epjst/e2009-01098-2.

Donges, J. F., Y. Zou, N. Marwan, and J. Kurths (Aug. 2009b). "The backbone of the climate network". In: *Europhysics Letters* 87.4, p. 48007. DOI: 10.1209/0295-5075/87/48007.

Donges, J. F., H. C. H. Schultz, N. Marwan, Y. Zou, and J. Kurths (Apr. 2011). "Investigating the topology of interacting networks". In: *The European Physical Journal B* 84.4, pp. 635–651. DOI: 10.1140/epjb/e2011-10795-8.

Donges, J. F., J. Heitzig, R. V. Donner, and J. Kurths (Apr. 2012). "Analytical framework for recurrence network analysis of time series". In: *Physical Review E* 85.4, p. 046105. DOI: 10.1103/PhysRevE.85.046105.

Donges, J. F., I. Petrova, A. Loew, N. Marwan, and J. Kurths (Jan. 2015a). "How complex climate networks complement eigen techniques for the statistical analysis of climatological data". en. In: *Climate Dynamics* 45.9-10, pp. 2407–2424. ISSN: 0930-7575. DOI: 10.1007/s00382-015-2479-3.

Donges, J. F., J. Heitzig, B. Beronov, M. Wiedermann, J. Runge, Q. Y. Feng, L. Tupikina, V. Stolbova, R. V. Donner, N. Marwan, H. A. Dijkstra, and J. Kurths

(Nov. 2015b). "Unified functional network and nonlinear time series analysis for complex systems science: The pyunicorn package". In: *Chaos* 25.11, p. 113101. DOI: 10.1063/1.4934554.

Donner, R. V., Y. Zou, J. F. Donges, N. Marwan, and J. Kurths (Mar. 2010). "Recurrence networks—a novel paradigm for nonlinear time series analysis". In: *New Journal of Physics* 12.3, p. 033025. DOI: 10.1088/1367-2630/12/3/033025.

Feng, A., Z. Gong, Q. Wang, and G. Feng (Feb. 2012). "Three-dimensional air–sea interactions investigated with bilayer networks". In: *Theoretical and Applied Climatology* 109.3-4, pp. 635–643. DOI: 10.1007/s00704-012-0600-7.

Feng, Q. Y. and H. Dijkstra (Jan. 2014). "Are North Atlantic multidecadal SST anomalies westward propagating?" In: *Geophysical Research Letters* 41.2, pp. 541–546. DOI: 10.1002/2013GL058687.

Feng, Q. Y., J. P. Viebahn, and H. A. Dijkstra (Aug. 2014). "Deep ocean early warning signals of an Atlantic MOC collapse". In: *Geophysical Research Letters* 41.16, pp. 6009–6015. DOI: 10.1002/2014GL061019.

Frankignoul, C. and N. Sennchael (Feb. 2007). "Observed Influence of North Pacific SST Anomalies on the Atmospheric Circulation". In: *Journal of Climate* 20.3, pp. 592–606. DOI: 10.1175/JCLI4021.1.

Frankignoul, C., G. de Coëtlogon, T. M. Joyce, and S. Dong (Dec. 2001). "Gulf Stream Variability and Ocean–Atmosphere Interactions". In: *Journal of Physical Oceanography* 31.12, pp. 3516–3529. DOI: 10.1175/1520-0485(2002)031<3516:GSVAOA>2.0.CO;2.

Gastineau, G. and C. Frankignoul (Feb. 2015). "Influence of the North Atlantic SST Variability on the Atmospheric Circulation during the Twentieth Century". In: *Journal of Climate* 28.4, pp. 1396–1416. DOI: 10.1175/JCLI-D-14-00424.1.

Ghil, M., M. R. Allen, M. D. Dettinger, K. Ide, D. Kondrashov, M. E. Mann, A. W. Robertson, A. Saunders, Y. Tian, F. Varadi, and P. Yiou (Feb. 2002). "Advanced Spectral Methods for Climatic Time Series". In: *Reviews of Geophysics* 40.1, p. 1003. DOI: 10.1029/2000RG000092.

Handorf, D. and K. Dethloff (2012). "How well do state-of-the-art atmosphere-ocean general circulation models reproduce atmospheric teleconnection patterns?" In: *Tellus A* 64. DOI: 10.3402/tellusa.v64i0.19777.

Handorf, D., R. Jaiser, K. Dethloff, A. Rinke, and J. Cohen (Apr. 2015). "Impacts of Arctic sea ice and continental snow cover changes on atmospheric winter teleconnections". In: *Geophysical Research Letters* 42.7, pp. 2367–2377. DOI: 10.1002/2015GL063203.

Hannachi, A., I. T. Jolliffe, and D. B. Stephenson (July 2007). "Empirical orthogonal functions and related techniques in atmospheric science: A review". In: *International Journal of Climatology* 27.9, pp. 1119–1152. DOI: 10.1002/joc.1499.

Heitzig, J., J. F. Donges, Y. Zou, N. Marwan, and J. Kurths (Jan. 2012). "Node-weighted measures for complex networks with spatially embedded, sampled, or differently sized nodes". In: *The European Physical Journal B* 85.1, 38. DOI: 10.1140/epjb/e2011-20678-7.

Hlinka, J., D. Hartman, N. Jajcay, M. Vejmelka, R. Donner, N. Marwan, J. Kurths, and M. Paluš (Apr. 2014). "Regional and inter-regional effects in evolving climate

networks". In: *Nonlinear Processes in Geophysics* 21.2, pp. 451–462. DOI: `10.5194/npg-21-451-2014`.

Kretschmer, M., D. Coumou, J. F. Donges, and J. Runge (2016). "Using Causal Effect Networks to Analyze Different Arctic Drivers of Midlatitude Winter Circulation". In: *Journal of Climate* 29.11, pp. 4069–4081. DOI: `10.1175/JCLI-D-15-0654.1`.

Kushnir, Y., W. A. Robinson, I. Blad, N. M. J. Hall, S. Peng, and R. Sutton (Aug. 2002). "Atmospheric GCM Response to Extratropical SST Anomalies: Synthesis and Evaluation". In: *Journal of Climate* 15.16, pp. 2233–2256. DOI: `10.1175/1520-0442(2002)015<2233:AGRTES>2.0.CO;2`.

Liu, Q., N. Wen, and Z. Liu (Sept. 2006). "An observational study of the impact of the North Pacific SST on the atmosphere". In: *Geophysical Research Letters* 33.18, p. L18611. DOI: `10.1029/2006GL026082`.

Ludescher, J., A. Gozolchiani, M. I. Bogachev, A. Bunde, S. Havlin, and H. J. Schellnhuber (July 2013). "Improved El Niño forecasting by cooperativity detection". In: *Proceedings of the National Academy of Sciences* 110.29, pp. 11742–11745. DOI: `10.1073/pnas.1309353110`.

Ludescher, J., A. Gozolchiani, M. I. Bogachev, A. Bunde, S. Havlin, and H. J. Schellnhuber (Feb. 2014). "Very early warning of next El Niño". In: *Proceedings of the National Academy of Sciences* 111.6, pp. 2064–2066. DOI: `10.1073/pnas.1323058111`.

Malik, N., N. Marwan, and J. Kurths (Sept. 2010). "Spatial structures and directionalities in Monsoonal precipitation over South Asia". In: *Nonlinear Processes in Geophysics* 17.5, pp. 371–381. DOI: `10.5194/npg-17-371-2010`.

Malik, N., B. Bookhagen, N. Marwan, and J. Kurths (Aug. 2011). "Analysis of spatial and temporal extreme monsoonal rainfall over South Asia using complex networks". In: *Climate Dynamics* 39.3-4, pp. 971–987. DOI: `10.1007/s00382-011-1156-4`.

Mheen, M. van der, H. A. Dijkstra, A. Gozolchiani, M. den Toom, Q. Feng, J. Kurths, and E. Hernandez-Garcia (June 2013). "Interaction network based early warning indicators for the Atlantic MOC collapse". In: *Geophysical Research Letters* 40.11, pp. 2714–2719. DOI: `10.1002/grl.50515`.

Molkenthin, N., K. Rehfeld, N. Marwan, and J. Kurths (Feb. 2014). "Networks from Flows - From Dynamics to Topology". In: *Scientific Reports* 4.4119. DOI: `10.1038/srep04119`.

Newman, M. (Jan. 2003). "The Structure and Function of Complex Networks". In: *SIAM Review* 45.2, pp. 167–256. DOI: `10.1137/S003614450342480`.

Paluš, M., D. Hartman, J. Hlinka, and M. Vejmelka (Oct. 2011). "Discerning connectivity from dynamics in climate networks". In: *Nonlin. Processes Geophys.* 18.5, pp. 751–763. DOI: `10.5194/npg-18-751-2011`.

Radebach, A., R. V. Donner, J. Runge, J. F. Donges, and J. Kurths (Nov. 2013). "Disentangling different types of El Niño episodes by evolving climate network analysis". In: *Physical Review E* 88.5, p. 052807. DOI: `10.1103/PhysRevE.88.052807`.

Ravasz, E., A. L. Somera, D. A. Mongru, Z. N. Oltvai, and A.-L. Barabási (Aug. 2002). "Hierarchical Organization of Modularity in Metabolic Networks". In: *Science* 297.5586, pp. 1551–1555. DOI: 10.1126/science.1073374.

Ravasz, E. and A.-L. Barabási (Feb. 2003). "Hierarchical organization in complex networks". In: *Physical Review E* 67.2, p. 026112. DOI: 10.1103/PhysRevE.67.026112.

Rayner, N. A., D. E. Parker, E. B. Horton, C. K. Folland, L. V. Alexander, D. P. Rowell, E. C. Kent, and A. Kaplan (July 2003). "Global analyses of sea surface temperature, sea ice, and night marine air temperature since the late nineteenth century". In: *Journal of Geophysical Research* 108.D14, p. 4407. DOI: 10.1029/2002JD002670.

Runge, J., J. Heitzig, N. Marwan, and J. Kurths (Dec. 2012). "Quantifying causal coupling strength: A lag-specific measure for multivariate time series related to transfer entropy". In: *Physical Review E* 86.6, p. 061121. DOI: 10.1103/PhysRevE.86.061121.

Runge, J., V. Petoukhov, and J. Kurths (Jan. 2014). "Quantifying the Strength and Delay of Climatic Interactions: The Ambiguities of Cross Correlation and a Novel Measure Based on Graphical Models". In: *Journal of Climate* 27.2, pp. 720–739. DOI: 10.1175/JCLI-D-13-00159.1.

Runge, J., V. Petoukhov, J. F. Donges, J. Hlinka, N. Jajcay, M. Vejmelka, D. Hartman, N. Marwan, M. Palu, and J. Kurths (Oct. 2015). "Identifying causal gateways and mediators in complex spatio-temporal systems". In: *Nature Communications* 6, p. 8502. DOI: 10.1038/ncomms9502.

Serreze, M. C. and J. A. Francis (Mar. 2006). "The Arctic Amplification Debate". In: *Climatic Change* 76.3-4, pp. 241–264. DOI: 10.1007/s10584-005-9017-y.

Steinhaeuser, K., A. R. Ganguly, and N. V. Chawla (June 2011). "Multivariate and multiscale dependence in the global climate system revealed through complex networks". In: *Climate Dynamics* 39.3-4, pp. 889–895. DOI: 10.1007/s00382-011-1135-9.

Stolbova, V., P. Martin, B. Bookhagen, N. Marwan, and J. Kurths (Aug. 2014). "Topology and seasonal evolution of the network of extreme precipitation over the Indian subcontinent and Sri Lanka". In: *Nonlinear Processes in Geophysics* 21.4, pp. 901–917. DOI: 10.5194/npg-21-901-2014.

Storch, H. von and F. W. Zwiers (2001). *Statistical Analysis in Climate Research*. Cambridge University Press. ISBN: 9780521012300.

Tantet, A. and H. A. Dijkstra (Jan. 2014). "An interaction network perspective on the relation between patterns of sea surface temperature variability and global mean surface temperature". In: *Earth System Dynamics* 5.1, pp. 1–14. DOI: 10.5194/esd-5-1-2014.

Tirabassi, G., C. Masoller, and M. Barreiro (Oct. 2015). "A study of the air-sea interaction in the South Atlantic Convergence Zone through Granger causality". en. In: *International Journal of Climatology* 35.12, pp. 3440–3453. ISSN: 08998418. DOI: 10.1002/joc.4218.

Trenberth, K. E. and J. W. Hurrell (Mar. 1994). "Decadal atmosphere-ocean variations in the Pacific". In: *Climate Dynamics* 9.6, pp. 303–319. DOI: 10.1007/BF00204745.

Tsonis, A. A. and P. J. Roebber (Feb. 2004). "The architecture of the climate network". In: *Physica A* 333, pp. 497–504. DOI: 10.1016/j.physa.2003.10.045.

Tsonis, A. A. and K. L. Swanson (June 2008). "Topology and Predictability of El Niño and La Niña Networks". In: *Physical Review Letters* 100.22, p. 228502. DOI: 10.1103/PhysRevLett.100.228502.

Tsonis, A. A., K. L. Swanson, and P. J. Roebber (May 2006). "What Do Networks Have to Do with Climate?" In: *Bulletin of the American Meteorological Society* 87.5, pp. 585–595. DOI: 10.1175/BAMS-87-5-585.

Tsonis, A. A., K. L. Swanson, and G. Wang (June 2008). "On the Role of Atmospheric Teleconnections in Climate". In: *Journal of Climate* 21.12, pp. 2990–3001. DOI: 10.1175/2007JCLI1907.1.

Tsonis, A. A., G. Wang, K. L. Swanson, F. A. Rodrigues, and L. d. F. Costa (July 2010). "Community structure and dynamics in climate networks". In: *Climate Dynamics* 37.5-6, pp. 933–940. DOI: 10.1007/s00382-010-0874-3.

Tupikina, L., K. Rehfeld, N. Molkenthin, V. Stolbova, N. Marwan, and J. Kurths (June 2014). "Characterizing the evolution of climate networks". In: *Nonlinear Processes in Geophysics* 21.3, pp. 705–711. DOI: 10.5194/npg-21-705-2014.

Uppala, S. M., P. W. Kållberg, A. J. Simmons, U. Andrae, V. D. C. Bechtold, M. Fiorino, J. K. Gibson, J. Haseler, A. Hernandez, G. A. Kelly, X. Li, K. Onogi, S. Saarinen, N. Sokka, R. P. Allan, E. Andersson, K. Arpe, M. A. Balmaseda, A. C. M. Beljaars, L. V. D. Berg, J. Bidlot, N. Bormann, S. Caires, F. Chevallier, A. Dethof, M. Dragosavac, M. Fisher, M. Fuentes, S. Hagemann, E. Hólm, B. J. Hoskins, L. Isaksen, P. a. E. M. Janssen, R. Jenne, A. P. Mcnally, J.-F. Mahfouf, J.-J. Morcrette, N. A. Rayner, R. W. Saunders, P. Simon, A. Sterl, K. E. Trenberth, A. Untch, D. Vasiljevic, P. Viterbo, and J. Woollen (Oct. 2005). "The ERA-40 re-analysis". In: *Quarterly Journal of the Royal Meteorological Society* 131.612, pp. 2961–3012. DOI: 10.1256/qj.04.176.

Vespignani, A. (Apr. 2010). "Complex networks: The fragility of interdependency". In: *Nature* 464.7291, pp. 984–985. DOI: 10.1038/464984a.

Wallace, J. M., Y. Zhang, and L. Bajuk (Feb. 1996). "Interpretation of Interdecadal Trends in Northern Hemisphere Surface Air Temperature". In: *Journal of Climate* 9.2, pp. 249–259. DOI: 10.1175/1520-0442(1996)009<0249:IOITIN>2.0.CO;2.

Wen, N., Z. Liu, Q. Liu, and C. Frankignoul (Dec. 2005). "Observations of SST, heat flux and North Atlantic Ocean-atmosphere interaction". In: *Geophysical Research Letters* 32.24, p. L24619. DOI: 10.1029/2005GL024871.

Wiedermann, M., J. F. Donges, J. Heitzig, and J. Kurths (2013). "Node-weighted interacting network measures improve the representation of real-world complex systems". In: *Europhysics Letters* 102.2, p. 28007. DOI: 10.1209/0295-5075/102/28007.

Wiedermann, M., A. Radebach, J. F. Donges, J. Kurths, and R. V. Donner (July 2016). "A climate network-based index to discriminate different types of El Nio and La Nia". In: *Geophys. Res. Lett.* 43.13, 2016GL069119. DOI: 10.1002/2016GL069119.

Woollings, T., A. Hannachi, and B. Hoskins (Apr. 2010). "Variability of the North Atlantic eddy-driven jet stream". In: *Quarterly Journal of the Royal Meteorological Society* 136.649, pp. 856–868. DOI: `10.1002/qj.625`.

Wyrtki, K. (Oct. 1975). "El Niño – The Dynamic Response of the Equatorial Pacific Oceanto Atmospheric Forcing". In: *Journal of Physical Oceanography* 5.4, pp. 572–584. DOI: `10.1175/1520-0485(1975)005<0572:ENTDRO>2.0.CO;2`.

Yamasaki, K., A. Gozolchiani, and S. Havlin (June 2008). "Climate Networks around the Globe are Significantly Affected by El Niño". In: *Physical Review Letters* 100.22, p. 228501. DOI: `10.1103/PhysRevLett.100.228501`.

Zemp, D. C., M. Wiedermann, J. Kurths, A. Rammig, and J. F. Donges (Sept. 2014). "Node-weighted measures for complex networks with directed and weighted edges for studying continental moisture recycling". In: *Europhysics Letters* 107.5, p. 58005. DOI: `10.1209/0295-5075/107/58005`.

Figure 1: Cross-threshold T_{si} between the subnetwork constructed from the SST field and all 18 isobaric surfaces of HGT in winter for different standard (unweighted) cross-link densities.
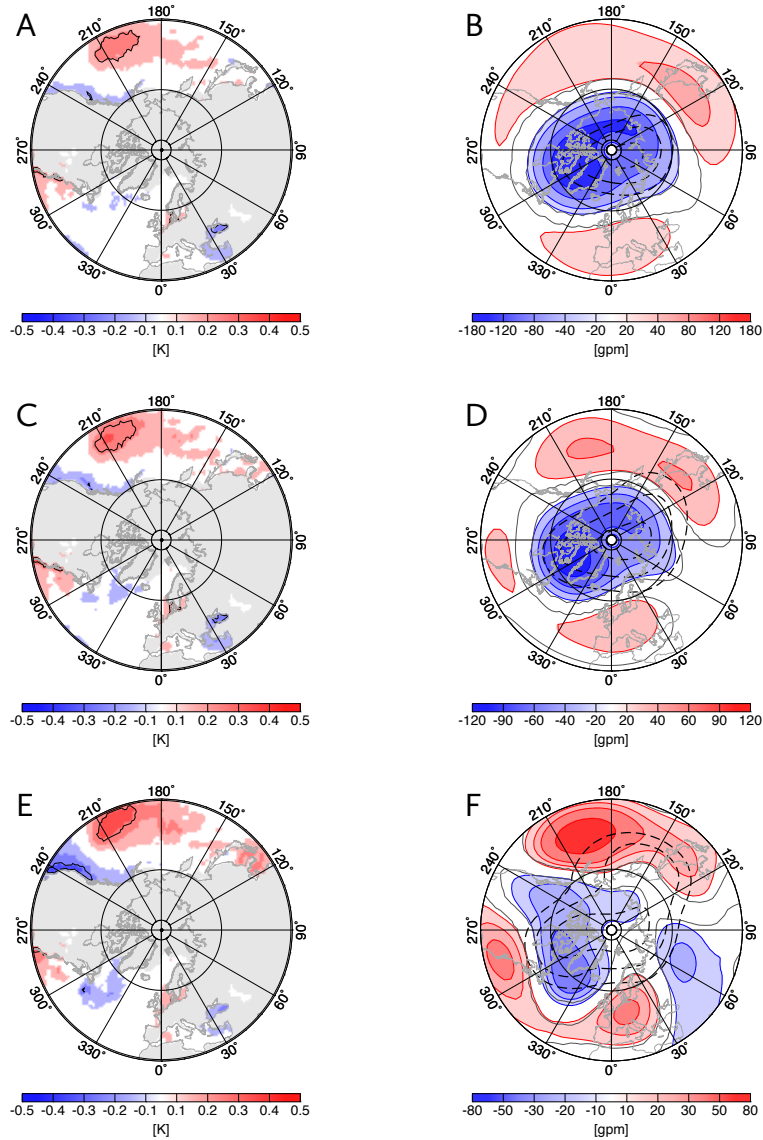
Figure 2: Leading coupled patterns obtained from MCA between the SST field and three layers of geopotential height at 50 mbar (A and B), 100 mbar (C and D) and 500 mbar (E and F) in winter (DJF). The left column (A, C and E) displays the component in the SST and the right column (B, D and F) that in the respective HGT field. All spatial patterns are shown as regression maps obtained by regressing SST anomalies and geopotential height anomalies onto associated time series for the geopotential height field for the respective MCA mode. Statistically significant areas at the 95% confidence level based on a two-tailed Student's t-test are shown as black contours (for the SST maps) and grey contours (for the geopotential height maps). Dashed lines indicate the climatic mean geopotential height fields.
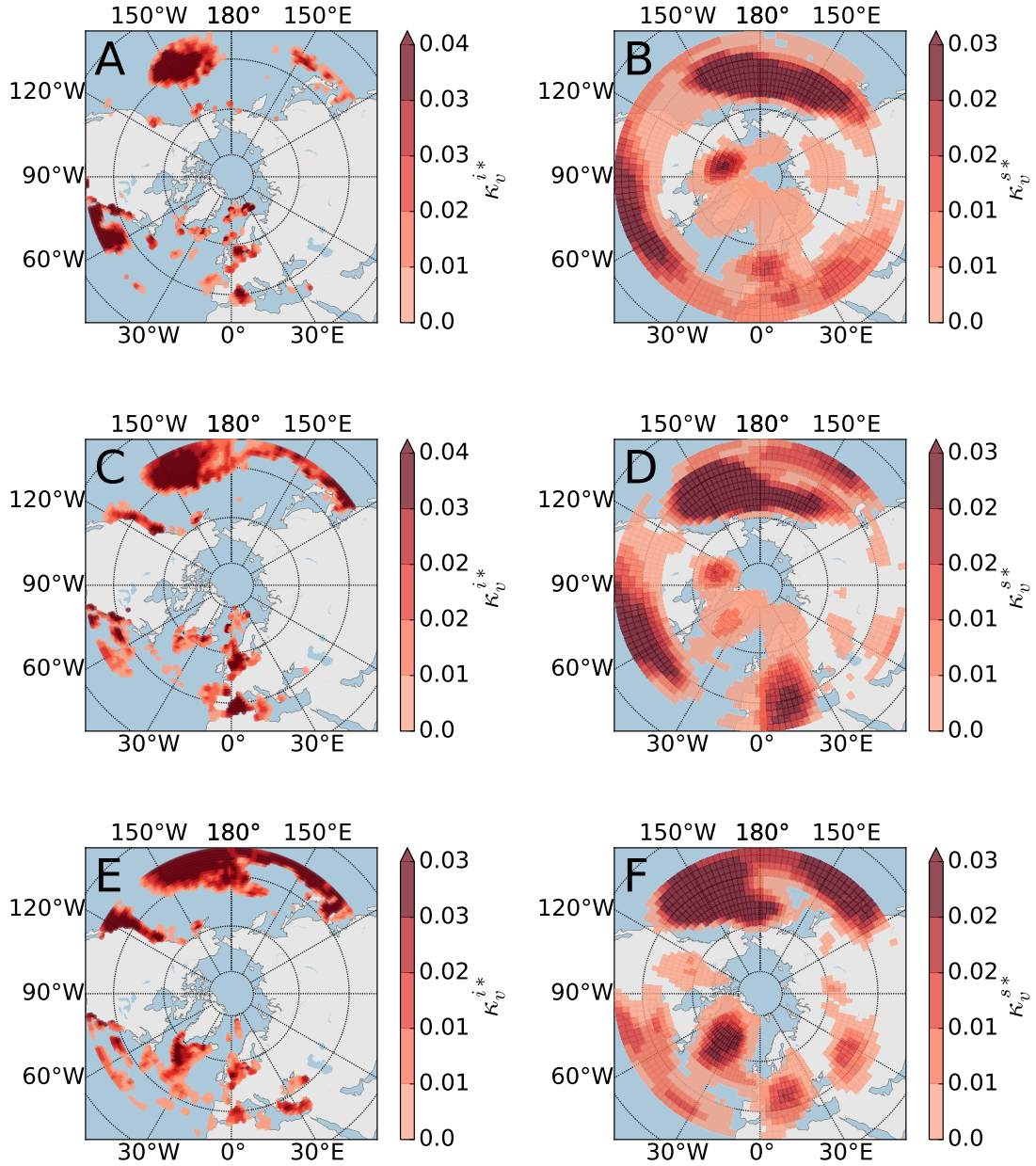
Figure 3: N.s.i. cross-degree density for coupled climate networks constructed from the SST field and three layers of geopotential height at 50 mbar (A and B), 100 mbar (C and D) and 500 mbar (E and F) for winter months (DJF). The left column (A, C and E) displays the n.s.i. cross degree density κ_v^{i*} for links pointing from the SST into the HGT subnetwork while the right column (B, D and F) displays the n.s.i. cross-degree density κ_v^{s*} for links pointing from the HGT into the SST subnetwork. Only nodes with $\kappa_v^{i*} > 0$ and $\kappa_v^{s*} > 0$ are shown.
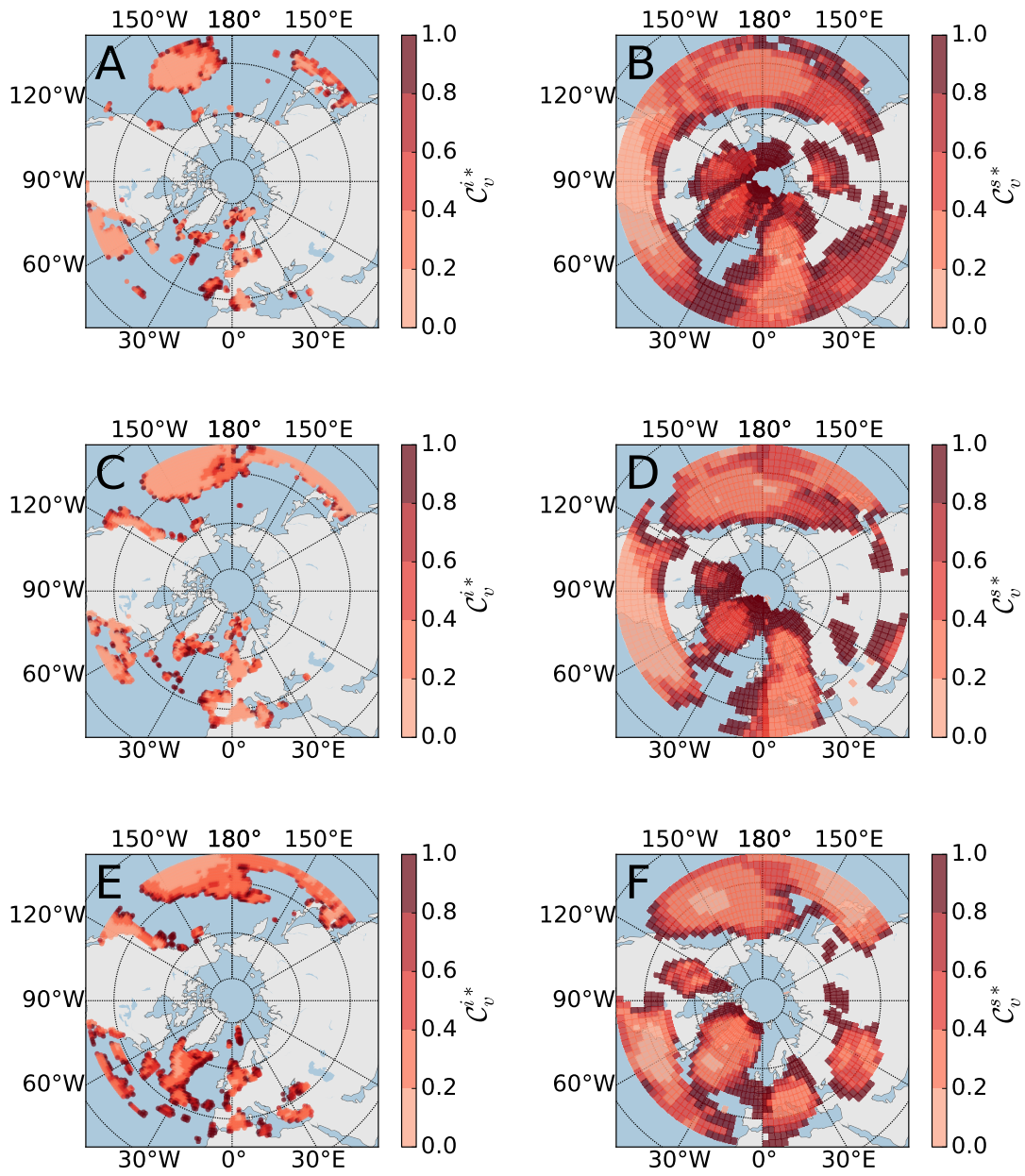
Figure 4: As in Fig. 3 for the n.s.i. local cross-clustering coefficients $\mathcal{C}_v^{i*}$ and $\mathcal{C}_v^{s*}$.
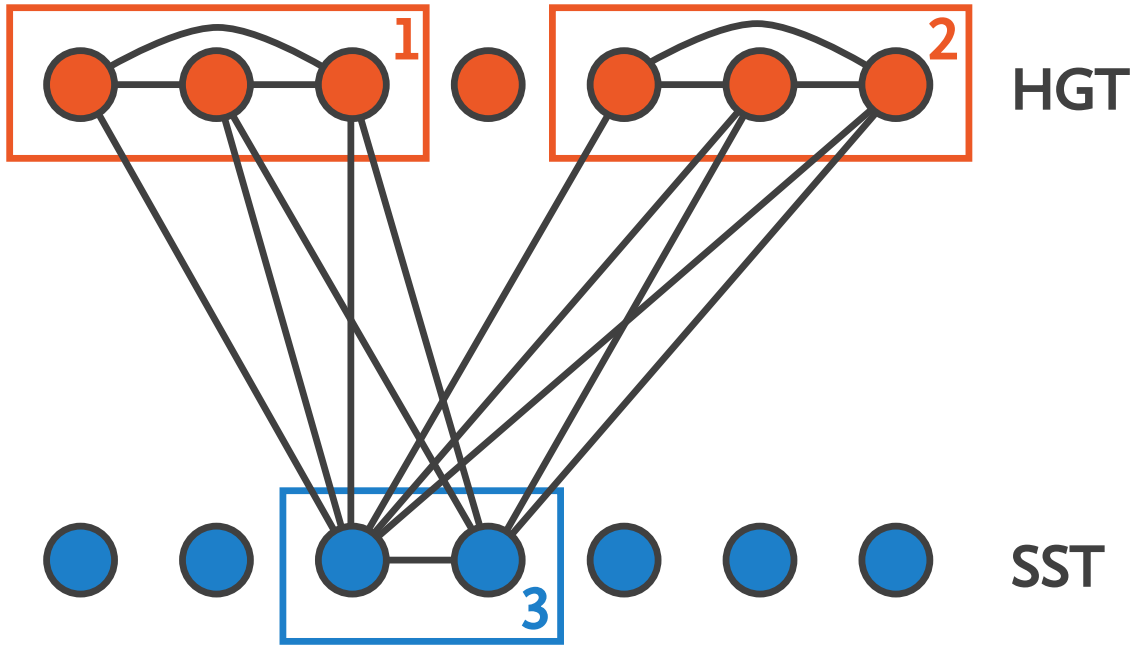
Figure 5: Schematic explanation of the observed quantitative differences in the n.s.i. local cross-clustering coefficients for nodes in the SST and HGT fields. Nodes in the ocean (box 3) tend to connect with statistically dissimilar and thus unconnected clusters of nodes in the atmosphere (such as nodes in box 1 and 2). Hence, the n.s.i. local cross-clustering coefficient $\mathcal{C}_v^{i*}$ only takes low values. In contrast, nodes in the atmosphere, e.g. from box 1, likely connect with clusters in the SST field, such as nodes exclusively in box 3. This results in a high n.s.i. cross local-clustering coefficient $\mathcal{C}_v^{s*}$ for nodes in the atmosphere.
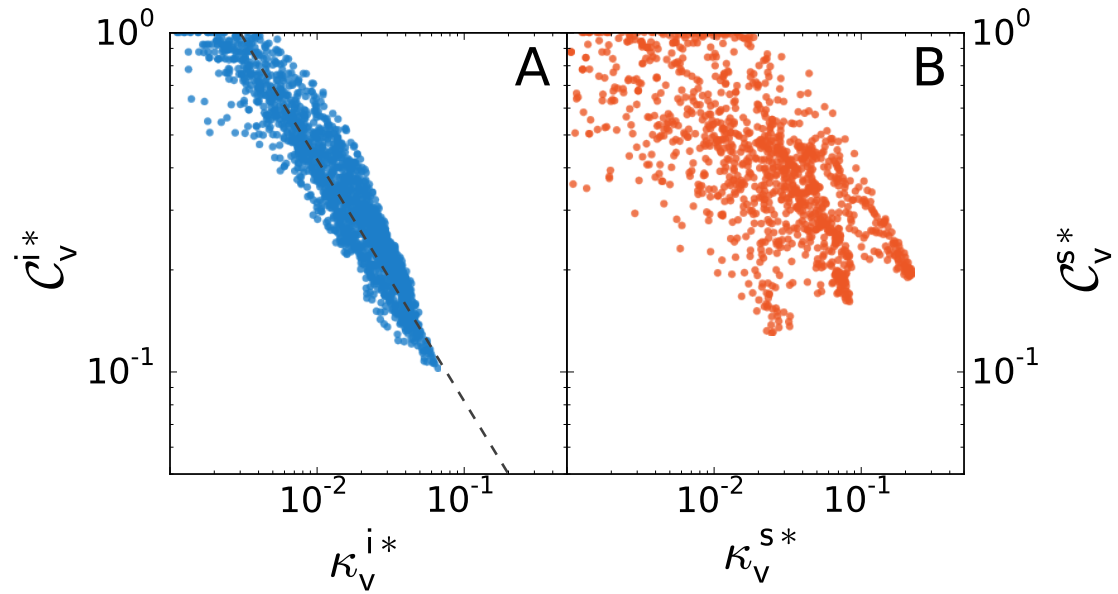
Figure 6: N.s.i. local cross-clustering coefficients $\mathcal{C}_v^{i*}(\kappa_v^{i*})$ for nodes in the SST field (A) and $\mathcal{C}_v^{s*}(\kappa_v^{s*})$ for nodes in the 500 mbar HGT field (B) as functions of the respective n.s.i. cross-degree densities. The dashed line in (A) indicates the relationship $\mathcal{C}_v^{i*} \sim (\kappa_v^{i*})^{-\alpha}$ (here with $\alpha = 0.94$) expected for traditional network measures $C_v(k_v)$ in the case of hierarchical network structures (Ravasz et al. 2002; Ravasz and Barabási 2003).
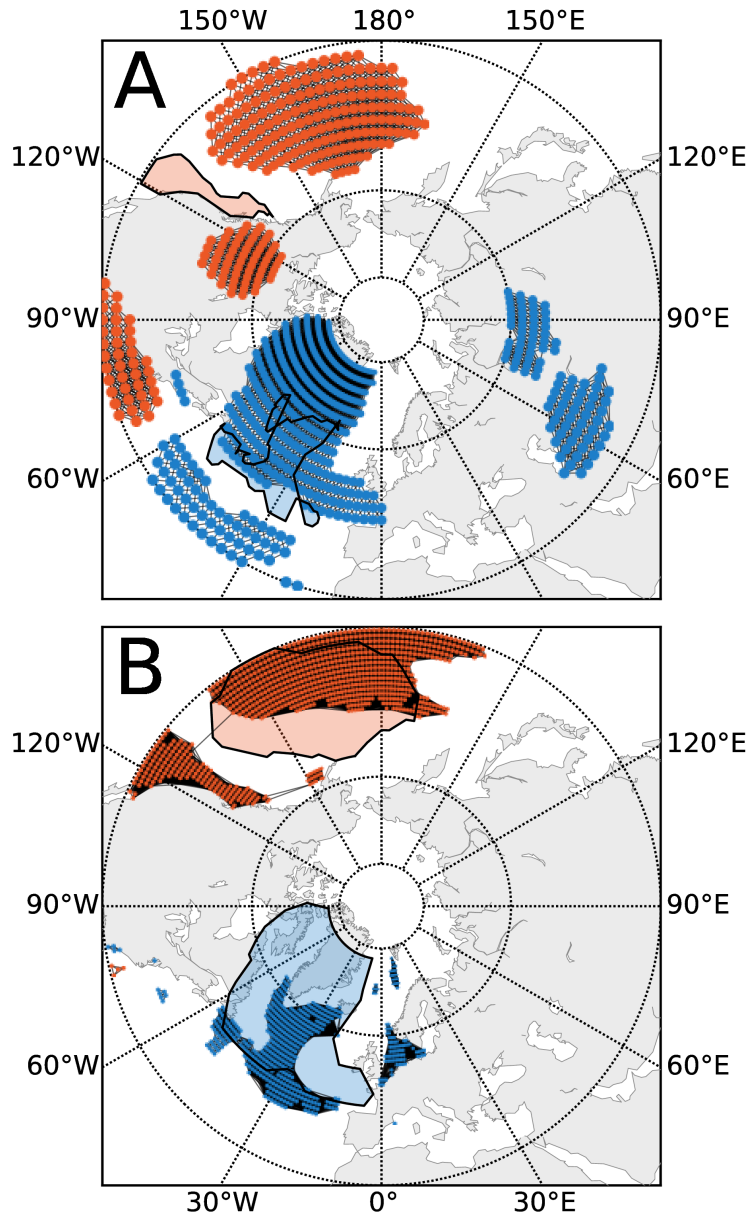
Figure 7: Visualization of a selection of nodes that are relevant for the observed hierarchical network structure. (A) Two clusters of nodes in the SST field (blue and orange shaded polygons) that show positive values of κ_v^{i*} with the 500 mbar HGT field (compare Fig. 3E). Correspondingly, coloured scatter points denote nodes in the HGT field that the considered SST nodes are connected with. All links that mutually connect the resulting HGT nodes are displayed as well. (B) The same for the two largest patches of nodes in the 500 mbar HGT field that where detected in (A). Coloured scatter points now indicate all nodes in the SST field that are connected with these patches.
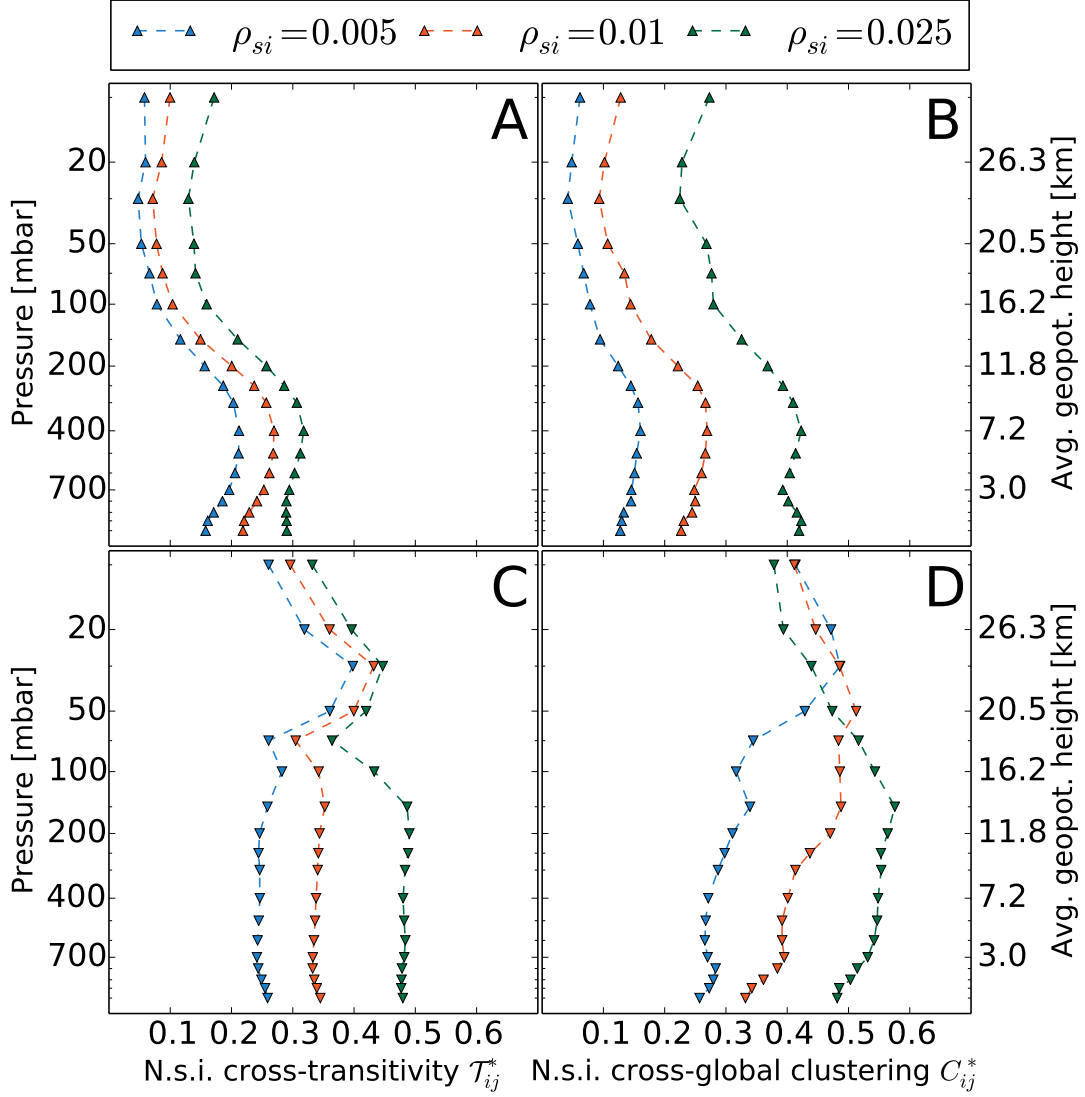
Figure 8: Global coupled network measures computed for all 18 coupled climate networks: (A) N.s.i. cross-transitivity and (B) n.s.i. global cross-clustering coefficient (B) taken over all nodes in the SST field. (C) and (D) display the respective measures computed over all nodes in the HGT field. To demonstrate the robustness and consistency of the results, we construct the networks for different choices of (unweighted) cross-link density ρ_{si} and internal link density $\rho_i = \rho_s = 2\rho_{si}$.

Table 1: Air pressure p_i and associated mean geopotential height Z_i as well as the internal threshold $T_i(\rho_{ii} = 0.01)$ corresponding to an internal link density of $\rho_{ii} = 0.01$ for each isobaric surface i.

Layer i	Air pressure p_i [mbar]	Geopotential height Z_i [km]	Threshold $T_i(\rho_{ii} = 0.01)$
0	10	30.9	0.9919
1	20	26.3	0.9936
2	30	23.7	0.9932
3	50	20.5	0.9876
4	70	18.4	0.9781
5	100	16.2	0.9621
6	150	13.7	0.9263
7	200	11.8	0.9166
8	250	10.4	0.8982
9	300	9.2	0.8894
10	400	7.2	0.8895
11	500	5.6	0.8958
12	600	4.2	0.9036
13	700	3.0	0.9119
14	775	2.2	0.9171
15	850	1.4	0.9205
16	925	0.8	0.9215
17	1000	0.1	0.9197